DNA Origami Nanopores for Controlling DNA Translocation

Silvia Hernández-Ainsa,[†,§] Nicholas A. W. Bell,[†,§] Vivek V. Thacker,[†,§] Kerstin Göpfrich,[†] Karolis Misiunas,[†] Maria Eugenia Fuentes-Perez,[‡] Fernando Moreno-Herrero,[‡] and Ulrich F. Keyser[†,*]

[†]Cavendish Laboratory, Department of Physics, University of Cambridge, JJ Thomson Avenue, Cambridge, CB3 0HE, United Kingdom and [‡]Department of Macromolecular Structures, Centro Nacional de Biotecnología, Consejo Superior de Investigaciones Científicas, Madrid, Spain. [§]S. Hernández-Ainsa, N. A. W. Bell, and V. V. Thacker contributed equally.

ABSTRACT We combine DNA origami structures with glass nanocapillaries to reversibly form hybrid DNA origami nanopores. Trapping of the DNA origami onto the nanocapillary is proven by imaging fluorescently labeled DNA origami structures and simultaneous ionic current measurements of the trapping events. We then show two applications highlighting the versatility of these DNA origami nanopores. First, by tuning the pore size we can control the folding of dsDNA molecules ("physical control"). Second, we show that the specific introduction of binding sites in the DNA origami nanopore allows selective detection of ssDNA as a function of the DNA sequence ("chemical control").

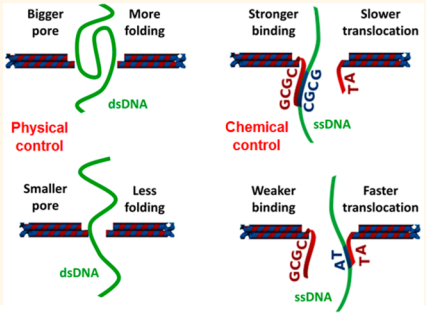

KEYWORDS: DNA structures · biosensors · fluorescent imaging · nanopores · nanotechnology

Scaffolded DNA origami[1] has emerged as a unique and versatile method to fabricate tailored nanostructures with a wide range of exciting applications in several scientific fields.[2−4] These include nanorobots capable of stimulating cell signaling for applications in biomedicine,[5,6] biomimetic systems to study motor protein transport in cells,[7] chiral plasmonic nanostructures with tunable optical response,[8] structures containing a cavity used for various biomolecular analyses such as enzymatic reactions,[9,10] G-quadruplex formation investigation[11] or protein capture,[12] and even functional single molecule nanopore biosensors.[13,14] The unique advantage of the DNA origami technique stems from the accurate control over the shape of the structure at the nanometer level that is easily achieved by harnessing the programmability of DNA base-pairing interactions.[15,16] This salient property is extremely valuable in the design and subsequent self-assembly of artificial systems in which nanometer control of shape and dimensions is required.

One recent example of nanostructures with a fundamental requirement of molecular control of shape and composition is synthetic nanopores made by silicon nanotechnology.[17] Although these systems have been successfully utilized for label-free single-molecule sensing, control of their internal architecture and surface is necessary to increase their specificity and sensitivity to various analytes.[18−20] Inspired by the recent demonstration of proteins incorporated into solid-state nanopores for single-molecule sensing,[21] the combination of DNA origami structures with solid-state nanopores promises an elegant and efficient alternative to achieve total control over the nanopore geometry and surface.[13,14,22] The formation of hybrid nanopores constituted by DNA origami and silicon nitride nanopores capable of detecting DNA[13] and proteins[14] has been recently reported. However, fabrication of silicon nitride nanopores is challenging and time-consuming, as it usually requires use of a transmission electron microscope (TEM) or focused ion beam to ablate the surface.[23] Glass nanocapillaries made by laser-assisted pipet pulling offer distinct advantages in terms of ease of manufacture without clean room facilities, orders of magnitude reduced cost, and enhanced throughput.[24,25] Our group has recently shown the possibility to form hybrid DNA origami nanopores with glass capillaries using multichannel devices.[26]

In this paper we go a step further, showing the possibility to form these hybrid DNA origami nanopores in a reversible

* Address correspondence to ufk20@cam.ac.uk.

Received for review April 10, 2013 and accepted June 4, 2013.

Published online June 04, 2013
10.1021/nn401759r

and repeated fashion by combining different DNA origami structures with glass nanocapillaries. We also verify the hybrid DNA origami nanopore formation using simultaneous ionic current and single-molecule fluorescence detection. We then demonstrate two applications highlighting the versatility of DNA origami nanopores: DNA translocation is controlled by varying the pore size ("physical control") or by using an oligonucleotide overhang–prey system ("chemical control").

RESULTS AND DISCUSSION

Glass nanocapillaries with an outer diameter of 46 ± 9 nm (see Figure S1 in the Supporting Information) were made by pulling glass capillaries with a laser-assisted pipet puller. The glass nanocapillaries were assembled into a polydimethylsiloxane device, schematically shown in Figure S2 (see Supporting Information).[24] To show the feasibility of combining DNA origami nanopores with glass nanocapillaries, we designed a flat DNA origami structure with outer dimensions of approximately 60 nm × 54 nm, two helices in height, and with a nanopore of 14 nm × 15 nm in the center (Figure 1a). In this design double-helical DNA domains were packed in a square lattice.[16] Structures were folded by mixing scaffold and staple strands in a 1:10 stoichiometric ratio and annealing the mixture over 18 h. Agarose gel electrophoresis of the purified DNA origami structures and atomic force microscopy (AFM) confirmed the formation of the designed structures with high yield (Figure 1b and Figure S3).

DNA origami nanopores were added to the reservoir containing the nanocapillary tip to a final concentration of 0.5 nM in a 1 M KCl/5.5 mM $MgCl_2$ solution buffered with 0.5 × TBE (pH = 8.2). A positive voltage applied in the back reservoir produced DNA origami trapping onto the nanocapillary, as expected.[13,14,26] We observe within a few seconds of applying a potential of 300 mV a drop in the ionic current and an increase in the current noise (current level "1" in Figure 1c and Figure S4 in the Supporting Information). This indicates the trapping of the DNA origami nanopore onto the glass nanocapillary and thus the formation of a hybrid DNA origami nanopore.[13,14,26] The small size of the glass nanocapillaries prevents translocations of the DNA origami structures. Interestingly, ejection of the DNA origami structure can be achieved by reversing the voltage to −1000 mV (current level "2" in Figure 1c). After ejection (current level "3" in Figure 1c), the initial current level is recovered. Such trapping and ejection (Figure 1d) was repeatedly performed over hundreds of times with the same glass nanocapillary without fouling. We observe a consistent percentage decrease in current upon trapping of DNA origami nanopores. The distribution is caused by different orientations of the DNA origami nanopores (Figure 1e). Some larger drops appear due to the presence of remaining DNA origami dimers or trimers even after filtration. The demonstrated reversibility and reproducibility

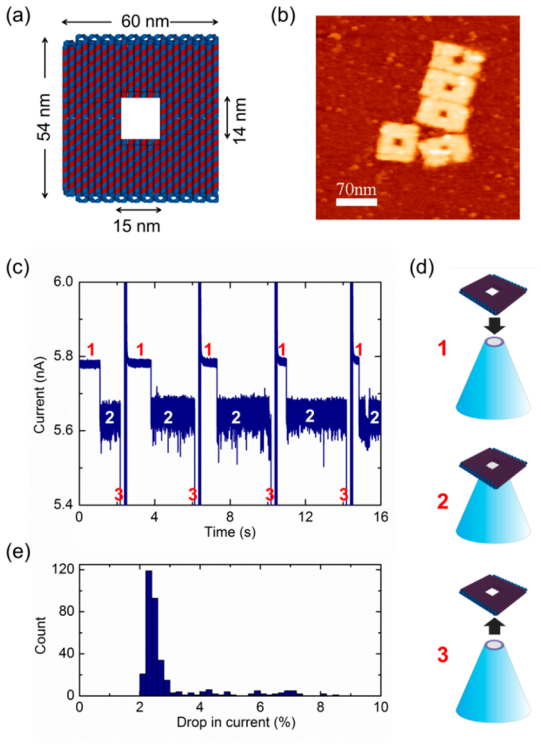

Figure 1. (a) Schematic representation of the DNA origami structure with a central 14 nm × 15 nm pore. (b) Topographic AFM image of assembled DNA origami structures deposited on mica and imaged in solution. (c) Ionic current trace showing reversible and repeated trapping and ejection of DNA origami on the glass nanocapillary ("14 nm" design). 1: Ionic current at 300 mV in the bare nanocapillary; 2: ionic current at 300 mV once the DNA origami has been trapped; 3: ionic current upon applying a negative voltage of −1000 mV (amplifier saturated). DNA origami was added at a concentration of 0.5 nM in the measurement buffer. (d) Schematic representation of the reversible DNA origami trapping and ejection on the glass nanocapillary corresponding to 1, 2, and 3 in (c), respectively. (e) Histogram of the percentage drop in ionic current produced by 352 "14 nm" DNA origami nanopore trapping events on one individual nanocapillary.

indicate the feasibility of combining DNA origami platforms with solid-state nanopores for highly sensitive and robust analyte detection.

To verify the successful trapping of the origami structures on a nanocapillary, we combined single-molecule fluorescence with ionic current detection using a custom-built setup previously described.[27] Staple strands with a Cy3 molecule attached on the 5′ end were used at six sites on the origami structure. The locations of the dye molecules are indicated in Figure 2a. Imaging was performed at 200 frames per second, and the fluorescently labeled origami structure was trapped onto the nanocapillary by a potential of 600 mV. A scheme of the setup is shown in Figure 2a along with a bright field image of the nanocapillary.

A DNA origami nanopore trapping is observed, indicated by the bright spot at the tip of the nanocapillary that appeared exactly when the ionic current

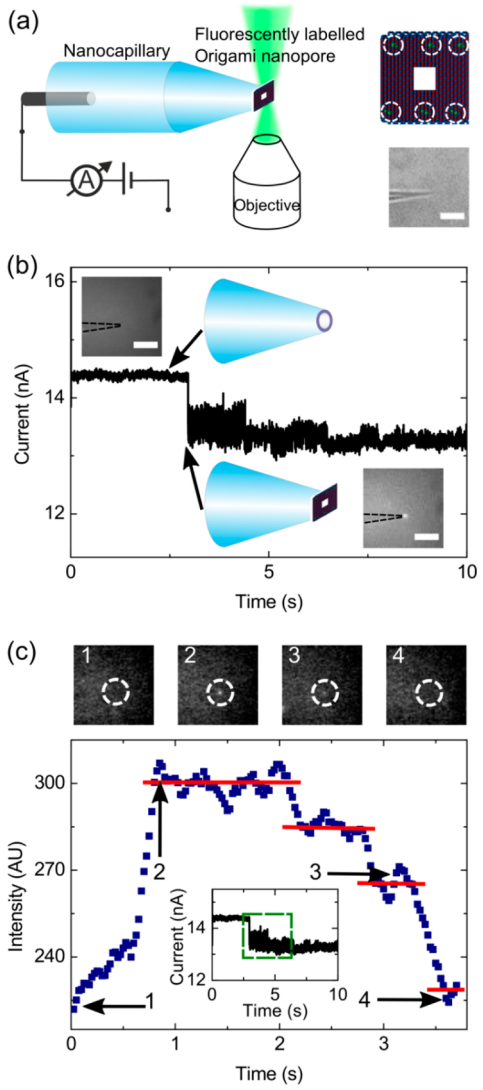

Figure 2. (a) Schematic representation of simultaneous fluorescence and ionic current detection using nanocapillaries. Cy3 dye molecules are attached at six sites on the 14 nm DNA origami design as indicated in green. Bright field image of the glass nanocapillary, scale bar = 5 μm. (b) Ionic current detection of origami nanopore trapping upon applying 600 mV. Images shown as insets in top-left and bottom-right corners are an average of 200 frames taken pretrapping (top) and post-trapping (bottom). (c) The DNA origami is pulled onto the glass nanocapillary (image 2) and then photobleaches in well-defined steps (images 3 and 4) evident from decreases in the pixel intensity at the nanocapillary tip. Each image shown is an average of 5 frames for clarity. The time interval in the ionic current trace where the photobleaching occurs is indicated by a green box (inset). Labeled DNA origami was added at a concentration of 0.1 nM in the measurement buffer.

decreased, as shown in Figure 2b (see Video 1 for the corresponding event in the Supporting Information). To improve the signal-to-noise ratio, images averaged over 200 frames before and after trapping of the DNA origami are shown as insets in Figure 2b. The hybrid origami nanopore can be discerned easily in the bottom inset. As expected, the trapped origami structure remained stable for tens of seconds, as indicated by the ionic current measurement (Figure 2b). However, the Cy3 fluorophores bleached within a few seconds in a stepwise fashion. This proves that the presence of a single DNA origami structure leads to the decrease in ionic current (Figure 2c). In order to elucidate this, Figure 2c shows the pixel intensity at the nanopore immediately before and after the origami trapping. Also shown are images (averaged over 5 frames) corresponding to labels 1−4 in the pixel intensity plot above the intensity time trace. The intensity increases from the baseline level pretrapping (image 1), and it is highest just at trapping (image 2). It then reduces (image 3) and returns back to the pretrapping intensity level (image 4). The discrete levels seen in the intensity are indicative of bleaching of individual Cy3 fluorophores.[28]

One of the most interesting characteristics of these DNA origami nanopores is the possibility to control the pore diameter by tuning the size of the pore in the DNA origami structure. This overcomes the limitations imposed by the small but inevitable variability in the diameter of the nanocapillaries and in any other semiconductor nanotechnology based nanopore. Furthermore, the incorporation of these DNA origami structures with nanocapillaries enables us to produce sub-10 nm diameter nanopores without the need for TEM drilling. Tuning the pore dimensions in the DNA origami structures is an ideal tool to control translocation of biomolecules. To this end, we investigated double-stranded λ-DNA folding occurring in DNA origami nanopores having different pore sizes. In particular we utilized the previously described structure with the 14 nm $\times$ 15 nm nanopore ("14 nm" design in the following) and another one with roughly the same overall dimensions but containing a significantly smaller nanopore of 5 nm $\times$ 7 nm ("5 nm" design) (Figure S5, Supporting Information). Hybrid nanopores with both DNA origami structures were formed as described before. Linear double-stranded λ-DNA (48.5 kbp) was then added to the same reservoir containing the DNA origami nanopores to a final concentration of 1 nM. Upon applying 500 mV, ionic current blockade events are observed due to the DNA translocation through the nanocapillary (Figure 3a, left). This happens due to the electrophoretic force that is exerted on the negatively charged DNA when applying a positive voltage. Events were observed as a decrease in the ionic current because the translocating DNA excludes ions from the nanopore.[24] The trapping of the DNA origami structures results in a drop in ionic current and the formation of the hybrid nanopore. λ-DNA translocation events are also observed in these hybrid nanopores (Figure 3a, right). Some characteristic λ-DNA ionic current blockades detected in both bigger and smaller hybrid DNA origami nanopores are shown in Figure 3b and c, respectively. The histograms of the whole ionic current trace during λ-DNA translocations in the bare (black) and in the hybrid

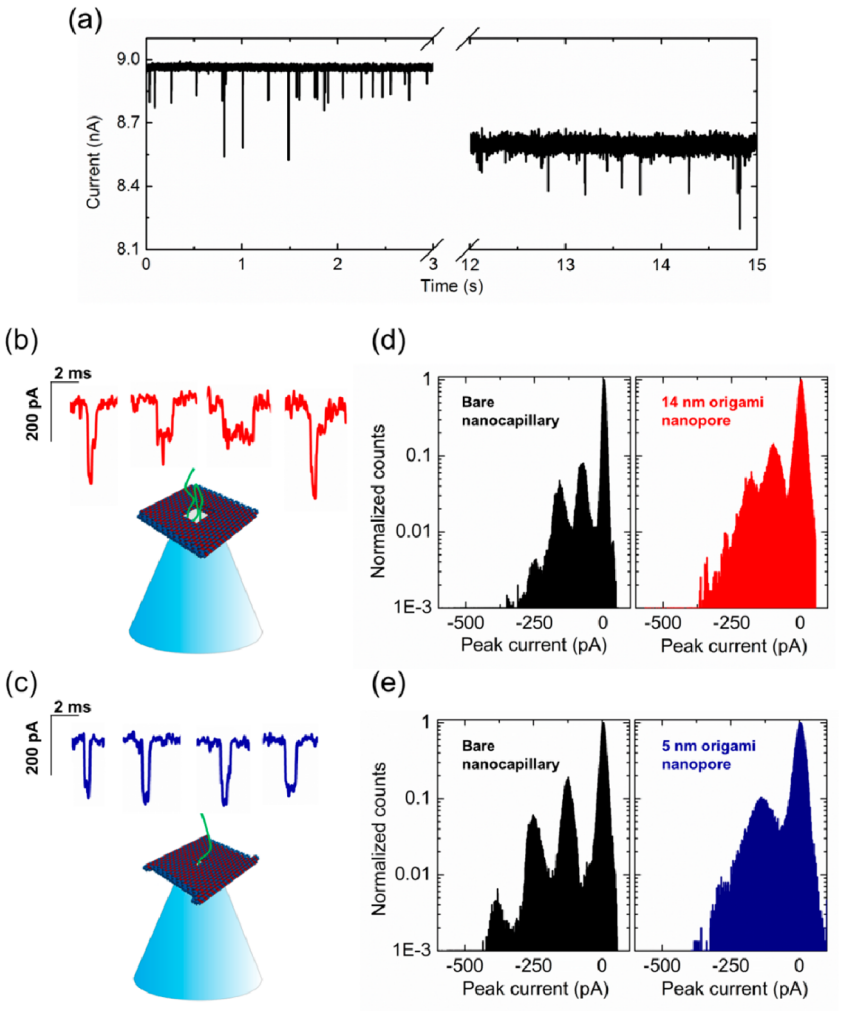

Figure 3. (a) Ionic current as a function of time upon applying 500 mV for an experiment with λ-DNA added to the reservoir to a final concentration of 1 nM in the measurement buffer. Initially λ-DNA translocations through the bare nanocapillary are detected. After the drop in ionic current the hybrid nanopore (14 nm design) is formed and λ-DNA translocations through the hybrid nanopore are also observed. (b and c) Typical λ-DNA translocation events for the 14 nm hybrid nanopore (red) and 5 nm hybrid nanopore (blue), respectively. The two experiments are also shown schematically (λ-DNA is represented as a green line). (d) Ionic current histograms of the DNA translocations for the bare nanocapillary (black) (326 events, peaks around −75, −160, and −250 pA) and the 14 nm hybrid nanopore formed after trapping of the DNA origami on the same nanocapillary (red) (190 events, peaks around −95, −180, −275, and −350 pA). (e) Same as in (d) but for a 5 nm hybrid nanopore: bare nanocapillary (black) (305 events, peaks around −125, −250, and −390 pA) and 5 nm hybrid nanopore (blue) (151 events, peaks around −145 and −300 pA). For each event the mean baseline current is subtracted before generating the histogram shown in (e) and (d). Peak around 0 pA corresponds to the open pore current. A different glass nanocapillary was used in (d) and (e).

nanopores (red and blue for the 14 nm and 5 nm DNA origami structures, respectively) are shown in Figure 3d and e. The existence of more than two peaks reveals λ-DNA folding, as expected.[24,29] Thus, DNA folding is clearly detected with the bare nanocapillaries.[24] However, the histograms for the hybrid nanopores differ depending on the size of the pore in the DNA origami design. Several peaks corresponding to different λ-DNA folding states are observed in the 14 nm design. By contrast, λ-DNA folding states are diminished in the 5 nm hybrid DNA origami nanopore. This result demonstrates convincingly not only that tailored origami nanopores can be used for robust sensing but also that the origami nanostructures sit in the correct orientation on the nanocapillary.

Apart from pore size control, DNA origami nanopores also enable the design of specific energy landscapes to chemically control the translocation of analytes. By specifically introducing binding sites in the DNA origami nanopore, we have created an artificial system capable of mimicking the selective passage of cargo molecules occurring in biological nanopores.[30] To demonstrate this, we extended two of the staple strands on either side of the nanopore, forming single-stranded DNA (ssDNA) overhangs with a specific "binding sequence" at the entrance of the 14 nm nanopore.[14] Thanks to the versatility of the DNA origami technique, we introduced two overhangs simultaneously in the same DNA origami structure in order to use the same

structure to detect a wider range of different preys. This is schematically shown in Figure 4a (top). As before, hybrid DNA origami nanopores were formed on nanocapillaries. Instead of λ-DNA, ssDNA "preys" (50 bases in length) with segments complementary to the binding sequence of the overhangs of the DNA origami nanopore were added to a final concentration of 500 nM. Translocations of the ssDNA preys through the hybrid DNA origami nanopore were recorded at 400 mV. At this potential, the trapping of the DNA origami nanopore worked reliably. A large increase in the translocation time of the ssDNA preys was observed due to the base pair interaction with the complementary DNA origami overhang, as schematically shown in Figure 4a (bottom). As shown in Figure 4b, we are able to detect binding interactions as switching of the ionic current between two distinct levels, indicating an unoccupied (level 1 in Figure 4a and b) or occupied binding site (level 2 in Figure 4a and b).

To prove the specificity of the binding sites, we vary both the length and sequence of the binding sequences introduced in the DNA origami nanopore. We observe a strong dependence of the event duration τ on the sequence of the ssDNA prey (Figure 4b). As shown in the current trace in Figure 4b as well as the events scatter plot in Figure 4c, the event duration for the $[T]_{23}CGCG[T]_{23}$ prey (complementary to the $[G]_3CGCG$ overhang) is about 1 order of magnitude longer than the one for the $[T]_{24}AT[T]_{24}$ prey (complementary to the $[T]_3AT$ overhang), indicating stronger interaction for the former sequence, as expected.

To gain insight in the transport characteristics of the interacting ssDNA through our DNA origami nanopore, we model our system as the ssDNA preys trapped in a potential well with an energy barrier of height W before translocation (inset Figure 4d). The dependence of event duration τ on W was tested for preys with four different sequences. For each overhang−prey combination, the mean event duration τ was experimentally determined and the binding potential W calculated.[31] As shown in Figure 4d, higher W results in longer event duration. Our experimental data can be accurately described using the Kramers' escape problem equation (eq 1).[32] For a potential well of depth W and curvature ω_a, the mean lifetime of the bound state (τ) is given by

$$\log \frac{1}{\tau} = -\frac{W}{kT} + \log \frac{{\omega_a}^2}{2\pi} \qquad (1)$$

Hence, the expected duration of the bound state can be related to W and the curvature of the potential (ω_a) (inset Figure 4d).

In our system, the well depth corresponds to the binding potential of double-stranded DNA and was calculated for each overhang−prey pair.[31] The mean lifetime is determined experimentally from the ionic current trace. As shown in Figure 4d, the model is a very good fit to the data.

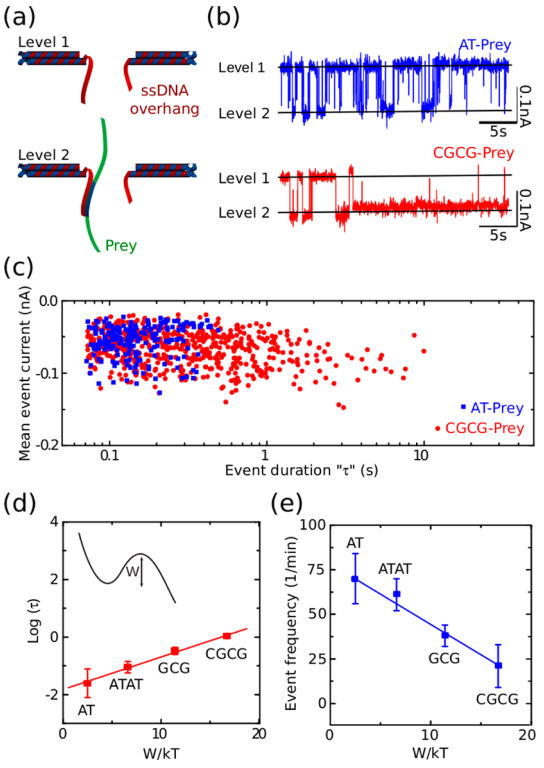

Figure 4. (a) Schematic cross section of the DNA origami design. The ssDNA overhangs (in red) are attached to the entrance of the nanopore of the 14 nm design and represent binding sites for complementary ssDNA preys (in green). Note that each overhang possesses a different sequence. (b) Ionic current traces for the translocation of $[T]_{24}AT[T]_{24}$ (upper panel) and $[T]_{23}CGCG[T]_{23}$ (bottom panel) preys. Preys were added to a final concentration of 500 nM in the measurement buffer. Translocations through the hybrid DNA origami nanopores were recorded at 400 mV. (c) Scatter plot of the mean event current amplitude and event duration (τ) for the $[T]_{24}AT[T]_{24}$ (blue) and $[T]_{23}CGCG[T]_{23}$ (red) preys. (d) Inverse log of the event duration τ as a function of binding potential. Four different preys ($[T]_{24}AT[T]_{24}$, $[T]_{23}ATAT[T]_{23}$, $[T]_{24}GCG[T]_{23}$, $[T]_{23}CGCG[T]_{23}$) were measured. The data were fitted using Kramers' escape problem for a particle exploring a potential landscape as shown in the inset graph. Error bars correspond to the standard deviation of the event duration within a 30 s interval for different origami trappings in the same nanocapillary. (e) Event frequency as a function of binding potential between overhangs and preys at 400 mV in 1 M KCl. A linear fit of all data points has been plotted to clarify this trend. Error bars correspond to the standard deviation of the number of events within a 30 s interval for different origami trappings in the same nanocapillary.

The transport characteristics of our DNA origami nanopore indicate that the transport through the pore strongly depends on the binding potential, as shown in Figure 4e. A strong binding site corresponds to long τ and thus smaller transport at high W. Our results on molecular transport agree qualitatively with experiments performed on microfluidic channels.[33]

CONCLUSION

In conclusion we have successfully created functional DNA origami nanopores by voltage trapping DNA origami on nanocapillaries. Using single-molecule

fluorescence imaging with simultaneous ionic current measurements, we present the first direct visualization of the trapping of DNA origami structures at the tip of the glass nanocapillaries. We have demonstrated the ability to influence folding of λ-DNA by tuning the pore diameter of the DNA origami structure. We have also proved the selectivity of this system to perform chemical detection of ssDNA as a function of the sequence.

Our nanocapillary−DNA origami system represents a remarkably simple method for the creation of tailored nanopores combining the high throughput and ease of manufacture of glass nanocapillaries and the vast possibilities of DNA nanotechnology.

MATERIALS AND METHODS

Glass Nanocapillary Device Fabrication. Quartz capillaries of outer diameter 0.5 mm, inner diameter of 0.2 mm, and a filament along the inside walls were purchased from Sutter. Capillaries were thoroughly cleaned by sonicating in acetone for 15 min and subsequently dried with gaseous nitrogen to remove any solvent. Then the capillaries were pulled using a laser-assisted pipet puller (Sutter P-2000). Once pulled, the nanocapillary was glued into a polydimethylsiloxane (PDMS) mold connecting two fluid reservoirs. The PDMS (Sylgard 184, Dow Corning) was made by mixing base and curing agent in a weight ratio of 10:1 and curing in a plastic mold for 24 h at 60 °C. The assembled device was plasma cleaned for 10 min (air plasma treatment at 100 W plasma power in a Femto-Diener Electronic plasma cleaner) to enhance the hydrophilicity of the nanocapillary walls. Immediately after, the reservoirs were filled with the required electrolyte, previously heated to 60 °C. All experiments were done utilizing 1 M KCl/5.5 mM $MgCl_2$ solution buffered with 0.5× TBE. The assembled cells were placed under vacuum to remove air bubbles. Silver wires (200 μm diameter, Advent) were chlorinated (Ag/AgCl) and inserted in both reservoirs.

DNA Origami Design, Assembly, and Purification. Structures were designed using the open source DNA origami software caDNAno.[34] Our designs consist of a double layer with 44 (5 nm pore design) or 48 (14 nm pore and fluorescently labeled designs) tightly interlinked double-helical DNA domains in a square packing lattice. The 7249 bases long viral M13mp18 ssDNA was utilized as scaffold (New England Biolabs), and all short ssDNA staples were purchased from Integrated DNA Technologies. A precise sequence of staples and the scaffold-staple layout for each design are gathered in the Supporting Information. DNA origami assembly was done by mixing scaffold and staples to a final concentration of 10 nM and 100 nM, respectively, in a 14 mM $MgCl_2$ solution buffered with 0.5 × TBE (pH = 8.2) and subjecting the mixture to thermal-annealing cycles for 18 h. The heating program utilized was as follows: 80 °C for 5 min, 79 °C for 4 min, from 79 to 60 °C in 19 steps (1 °C per step, 4 min each step), keep at 60 °C for 30 min, from 60 to 25 °C in 35 steps (1 °C per step, 30 min each step), and finally set at 4 °C. The assembled structures were purified from the excess staple strands by centrifugation with 100 kDa MWCO filters (Amicon Ultra, Millipore) in three cycles at a speed of 13000*g* for 5 min at 4 °C with an 11 mM $MgCl_2$ solution buffered with 0.5× TBE added to the filter column at the beginning of each cycle. The filter was then turned upside down, and the DNA origami collected by spinning for 2 min at 1000*g*. In the case of the fluorescently labeled DNA origami structures, the assembly and purification processes were done avoiding light exposure to reduce fluorophore bleaching.

DNA Origami Characterization. The folding quality of the already purified DNA origami structures was analyzed by agarose gel electrophoresis. Agarose gels (1.5%) in a 11 mM $MgCl_2$ solution buffered with 0.5× TBE (pH = 8.2) were run at 80 V for 3 h in a gel box externally cooled with an ice water bath. Ethidium bromide (0.5 μg/mL) was utilized to stain DNA origami structures in the gel. Atomic force microscopy measurements were performed in tapping mode with Olympus TR400-PSA tips (spring constant 0.08 N/m). The scan rate was 1 Hz (512 points). Samples were deposited on freshly cleaved mica and imaged in solution (10 mM $MgCl_2$, 2 mM $NiCl_2$, 40 mM NaCl) buffered with 10 mM Tris-HCl (pH = 8.0).

Ionic Current Data Acquisition. Ionic current measurements were performed using an Axopatch 200B (Axon Instruments, USA) amplifier in voltage-clamp mode. Ionic current was recorded at 100 kHz bandwidth with the internal Bessel filter of the amplifier at 10 kHz. All signals were digitized with a NI-PCIe-6251card (National Instruments, USA). Custom written LabVIEW (LabVIEW 8.6, National Instruments) programs were used to record and process all data.

DNA Origami Fluorescent Imaging. The fluorescently labeled DNA origami structures were excited by emissions from a 532 nm laser (Laser Quantum) operating at <5 mW. A long pass dichroic mirror at 532 nm (Semrock Filters) directed the excitation light to the rear of a 60× objective (UPLSAPO NA.1.2, Olympus). The fluorescence emission from the fluorophores was collected *via* the same objective, passed through the dichroic mirror, and focused *via* a mirror and a tube lens to the sensor of a fast electron multiplying CCD camera (Andor iXON3 860). Data acquisition for both ionic current and fluorescence images is done through custom software written in LABVIEW and a DAQ card (PCIe-6351, National Instruments).

λ-DNA Translocation Experiments. Linear double-stranded λ-DNA (48.5 kbp) stock solution (Fermentas, 300 μg/mL) was diluted to 1 nM in the measurement solution (1 M KCl, 5.5 mM $MgCl_2$ buffered with 0.5 × TBE). λ-DNA translocations through both the bare and the hybrid DNA origami nanopores were driven by applying 500 mV.

ssDNA Translocation Experiments. Single-stranded DNA preys (Integrated DNA Technologies, 50nt, 100 μM in 1× TE buffer, pH 8) were diluted to 500 nM in the measurement solution (1 M KCl, 5.5 mM $MgCl_2$ buffered with 0.5× TBE). Translocations through the hybrid DNA origami nanopores were recorded at 400 mV.

Conflict of Interest: The authors declare no competing financial interest.

Supporting Information Available: SEM image of glass nanocapillary, schematic representation of the devices, agarose gel and AFM images of purified DNA origami structures, ionic current noise analysis in bare and hybrid nanopore, additional ionic current traces of DNA origami trapping, staple strand sequences of DNA origami structure, video showing ionic current and single-molecule fluorescence detection of DNA origami nanopore trapping, scaffold-staple layout for each DNA origami structure. This material is available free of charge *via* the Internet at http://pubs.acs.org.

Acknowledgment. S.H.A. and U.F.K. acknowledge support from an ERC starting grant and from Oxford Nanopore Technologies (www.nanoporetech.com). N.A.W.B. was supported by the EPSRC NanoDTC program. V.V.T. gratefully acknowledges funding from the Cambridge Commonwealth Trust, the Jawaharlal Nehru Memorial Trust, and the Emmy Noether program. K.G. acknowledges support from the German National Academic Foundation. K.M. was supported by the EPSRC program. Work in the FMH laboratory was supported by a Starting Grant from the European Research Council (no. 206117) and a grant from the Spanish Ministry of Economy and Competitiveness (FIS2011-24638). M.E.F.P. acknowledges support by a contract from CSIC (contract number 200920I123).

REFERENCES AND NOTES

1. Rothemund, P.W. K. Folding DNA to Create Nanoscale Shapes and Patterns. *Nature* **2006**, *440*, 297–302.

2. Pinheiro, A. V.; Han, D.; Shih, W. M.; Yan, H. Challenges and Opportunities for Structural DNA Nanotechnology. *Nat. Nanotechnol.* **2011**, *6*, 763–772.
3. Tørring, T.; Voigt, N. V.; Nangreave, J.; Yan, H.; Gothelf, K. V. DNA Origami: A Quantum Leap for Self-Assembly of Complex Structures. *Chem. Soc. Rev.* **2011**, *40*, 5636–5646.
4. Rajendran, A.; Endo, M.; Sugiyama, H. Single-Molecule Analysis Using DNA Origami. *Angew. Chem., Int. Ed.* **2012**, *51*, 874–890.
5. Elbaz, J.; Willner, I. DNA Origami: Nanorobots Grab Cellular Control. *Nat. Mater.* **2012**, *11*, 276–277.
6. Douglas, S. M.; Bachelet, I.; Church, G. M. A Logic-Gated Nanorobot for Targeted Transport of Molecular Payloads. *Science* **2012**, *335*, 831–834.
7. Derr, N. D.; Goodman, B. S.; Jungmann, R.; Leschziner, A. E.; Shih, W. M.; Reck-Peterson, S. L. Tug-of-War in Motor Protein Ensembles Revealed with a Programmable DNA Origami Scaffold. *Science* **2012**, *338*, 662–665.
8. Kuzyk, A.; Schreiber, R.; Fan, Z.; Pardatscher, G.; Roller, E. M.; Högele, A.; Simmel, F. C.; Govorov, A. O.; Liedl, T. DNA-Based Self-Assembly of Chiral Plasmonic Nanostructures with Tailored Optical Response. *Nature* **2012**, *483*, 311–314.
9. Endo, M.; Katsuda, Y.; Hidaka, K.; Sugiyama, H. Regulation of DNA Methylation Using Different Tensions of Double Strands Constructed in a Defined DNA Nanostructure. *J. Am. Chem. Soc.* **2010**, *132*, 1592–1597.
10. Endo, M.; Katsuda, Y.; Hidaka, K.; Sugiyama, H. A Versatile DNA Nanochip for Direct Analysis of DNA Base-Excision. *Angew. Chem., Int. Ed.* **2010**, *49*, 9412–9416.
11. Sannohe, Y.; Endo, M.; Katsuda, Y.; Hidaka, K.; Sugiyama, H. Visualization of Dynamic Conformational Switching of the G-Quadruplex in a DNA Nanostructure. *J. Am. Chem. Soc.* **2010**, *132*, 16311–16313.
12. Kuzuya, A.; Kimura, M.; Numajiri, K.; Koshi, N.; Ohnishi, T.; Okada, F.; Komiyama, M. Precisely Programmed and Robust 2D Streptavidin Nanoarrays by Using Periodical Nanometer Scale Wells Embedded in DNA Origami Assembly. *ChemBioChem* **2009**, *10*, 1811–1815.
13. Bell, N. A. W.; Engst, C. R.; Ablay, M.; Divitini, G.; Ducati, C.; Liedl, T.; Keyser, U. F. DNA Origami Nanopores. *Nano Lett.* **2012**, *12*, 512–517.
14. Wei, R.; Martin, T. G.; Rant, U.; Dietz, H. DNA Origami Gatekeepers for Solid-State Nanopores. *Angew. Chem., Int. Ed.* **2012**, *51*, 4864–4867.
15. Douglas, S. M.; Dietz, H.; Liedl, T.; Högberg, B.; Graf, F.; Shih, W. M. Self-Assembly of DNA into Nanoscale Three-Dimensional Shapes. *Nature* **2009**, *459*, 414–418.
16. Castro, C. E.; Kilchherr, F.; Kim, D. N.; Shiao, E. L.; Wauer, T.; Wortmann, P.; Bathe, M.; Dietz, H. A Primer to Scaffolded DNA Origami. *Nat. Methods* **2011**, *8*, 221–229.
17. Keyser, U. F. Controlling Molecular Transport through Nanopores. *J. R. Soc. Interface* **2011**, *8*, 1369–1378.
18. Yusko, E. C.; Prangkio, P.; Sept, D.; Rollings, R. C.; Li, J.; Mayer, M. Single-Particle Characterization of Aβ Oligomers in Solution. *ACS Nano* **2012**, *6*, 5909–5919.
19. Yusko, E. C.; Johnson, J. M.; Majd, S.; Prangkio, P.; Rollings, R. C.; Li, J.; Yang, J.; Mayer, M. Controlling Protein Translocation through Nanopores with Bio-Inspired Fluid Walls. *Nat. Nanotechnol.* **2011**, *6*, 253–260.
20. Hernández-Ainsa, S.; Muus, C.; Bell, N. A. W.; Steinbock, L. J.; Thacker, V. V.; Keyser, U. F. Lipid-Coated Nanocapillaries for DNA Sensing. *Analyst* **2013**, *138*, 104–106.
21. Hall, A. R.; Scott, A.; Rotem, D.; Mehta, K. K.; Bayley, H.; Dekker, C. Hybrid Pore Formation by Directed Insertion of α-Haemolysin into Solid-State Nanopores. *Nat. Nanotechnol.* **2010**, *5*, 874–877.
22. Langecker, M.; Arnaut, V.; Martin, T. G.; List, J.; Renner, S.; Mayer, M.; Dietz, H.; Simmel, F. C. Synthetic Lipid Membrane Channels Formed by Designed DNA Nanostructures. *Science* **2012**, *338*, 932–936.
23. Li, J.; Stein, D.; McMullan, C.; Branton, D.; Aziz, M. J.; Golovchenko, J. A. Ion-Beam Sculpting at Nanometre Length Scales. *Nature* **2001**, *412*, 166–169.
24. Steinbock, L. J.; Otto, O.; Chimerel, C.; Gornall, J. L.; Keyser, U. F. Detecting DNA Folding with Nanocapillaries. *Nano Lett.* **2010**, *10*, 2493–2497.
25. Morris, C. A.; Friedman, A. K.; Baker, L. A. Applications of Nanopipettes in the Analytical Sciences. *Analyst* **2010**, *135*, 2190–2202.
26. Bell, N. A. W.; Thacker, V. V.; Hernández-Ainsa, S.; Fuentes-Perez, M. E.; Moreno-Herrero, F.; Liedl, T.; Keyser, U. F. Multiplexed Ionic Current Sensing with Glass Nanopores. *Lab Chip* **2013**, *13*, 1859–1862.
27. Thacker, V. V.; Ghosal, S.; Hernández-Ainsa, S.; Bell, N. A. W.; Keyser, U. F. Studying DNA Translocation in Nanocapillaries Using Single Molecule Fluorescence. *Appl. Phys. Lett.* **2012**, *101*, 223704–4.
28. Gordon, M. P.; Ha, T.; Selvin, P. R. Single-Molecule High-Resolution Imaging with Photobleaching. *Proc. Natl. Acad. Sci. U.S.A.* **2004**, *101*, 6462–6465.
29. Li, J.; Gershow, M.; Stein, D.; Brandin, E.; Golovchenko, J. A. DNA Molecules and Configurations in a Solid-State Nanopore Microscope. *Nat. Mater.* **2003**, *2*, 611–615.
30. Alberts, B.; Johnson, A.; Lewis, J.; Raff, M.; Roberts, K.; Walter, P. B. *Molecular Biology of the Cell*, 5th ed.; Garland Science, 2008.
31. Binding potentials were calculated using the SciTools provided in the Integrated DNA Technology (IDT) webpage, http://eu.idtdna.com/pages/scitools.
32. Kramers, H. A. Brownian Motion in a Field of Force and the Diffusion Model of Chemical Reactions. *Physica (Utrecht)* **1940**, *7*, 284–304.
33. Pagliara, S.; Schwall, C.; Keyser, U. F. Optimizing Diffusive Transport through a Synthetic Membrane Channel. *Adv. Mater.* **2013**, *25*, 844–849.
34. Douglas, S. M.; Marblestone, A. H.; Teerapittayanon, S.; Vazquez, A.; Church, G. M.; Shih, W. M. Rapid Prototyping of 3D DNA-Origami Shapes with caDNAno. *Nucleic Acids Res.* **2009**, *37*, 5001–5006.